Published in final edited form as:
Mol Cancer Res. 2014 January ; 12(1): 82–90. doi:10.1158/1541-7786.MCR-13-0392.

Loss of the nucleosome-binding protein HMGN1 affects the rate of N-nitrosodiethylamine induced hepatocarcinogenesis in mice

Yuri V. Postnikov[1,*], **Takashi Furusawa**[1], **Diana C. Haines**[2], **Valentina M. Factor**[3], and **Michael Bustin**[1]

[1]Laboratory of Metabolism, National Cancer Institute, National Institutes of Health, Bethesda, MD 20852

[2]Science Applications International Corporation, National Cancer Institute-Frederick, National Institutes of Health, Frederick, MD 21702

[3]National Institutes of Health, National Cancer Institute, Laboratory of Experimental Carcinogenesis, Bethesda, MD 20852

Abstract

We report that HMGN1, a nucleosome binding protein that affects chromatin structure and function, affects the growth of N-nitrosodiethylamine (DEN) induced liver tumors. Following a single DEN injection at 2 weeks of age, *Hmgn1*$^{tm1/tm1}$ mice, lacking the nucleosome-binding domain of HMGN1, had earlier signs of liver tumorigenesis than their *Hmgn1*$^{+/+}$ littermates. Detailed gene expression profiling revealed significant differences between DEN-injected and control saline injected mice, but only minor differences between the injected *Hmgn1*$^{tm1/tm1}$ mice and their *Hmgn1*$^{+/+}$ littermates. Pathway analysis revealed that the most significant process affected by loss of HMGN1 involves the lipid/ sterol metabolic pathway. Our study indicates that in mice, loss of HMGN1 leads to transcription changes that accelerate the progression of DEN-induced hepatocarcinogenesis, without affecting the type of tumors or the final total tumor burden of these mice.

Introduction

The dynamic properties of the chromatin fiber play a key role in transcriptional regulation and in the establishment and maintenance of epigenetic marks. Disruption of these processes can alter gene expression, potentially leading to various diseases including cancer. Indeed, increasing evidence links misexpression of tumor suppressors and oncogenes, and disregulation of DNA repair processes, to alterations in chromatin structure and to changes in epigenetic marks such as covalent modification in DNA and histones (1–3). Factors that affect epigenetic marks in the genome have been shown to contribute to the progression of cancer (4) and epigenetic drugs targeting chromatin regulators show promise as anticancer agents (5). Because any factor that affects epigenetic processes could potentially contribute to tumorigenicity, it is important to examine the role of various chromatin modifiers in the etiology of cancer. Here we investigate the potential role of the chromatin binding protein high mobility group N1 (HMGN1) in hepatocarcinogenesis.

HMGN1 is a member of the high mobility group N (HMGN) family of chromosomal proteins. HMGN proteins are ubiquitously present in the nuclei of vertebrate cells and bind

[*]To whom correspondence should be addressed. Tel: +1 301 496 2885; Fax: +1 301 496 8419; postniky@mail.nih.gov.

Conflict of Interest Statement: None declared

specifically to nucleosome core particles, the building block of the chromatin fiber (6). The chromatin residence time of all HMGNs is short, these proteins continuously roam throughout the nucleus and reside only transiently on a specific site (7). Although HMGNs can interact with all nucleosomes, their genome wide organization is not random. Chromatin immunoprecipiation studies revealed that HMGN1 preferentially binds to gene promoters and enhancers where they tend to colocalize with DNase I hypersensitive sites, a hallmark of chromatin regulatory sites (8).

The binding of HMGN1 to nucleosomes induces structural changes in chromatin and alters the levels of posttranslational modifications of core histones raising the possibility that HMGN1 affects epigenetic regulatory processes. Significantly, the effects of HMGN1 on chromatin structure and function are contingent on the ability of the protein to bind to nucleosomes, HMGN1 mutants that do not bind to nucleosomes do not affect chromatin structure or histone modifications (9–13). We have generated the mice lacking functional HMGN1 (*Hmgn1*$^{tm1/tm1}$ mice, formerly named *Hmgn1*$^{-/-}$), that has been considered as *Hmgn1* knockout mice, although the mice express heavily truncated HMGN1 that does not localize to nucleus. Studies with cells and tissues derived from genetically altered HMGN1 mice, that express HMGN1 mutant that cannot bind to nucleosomes revealed that loss of HMGN1 function alters the cellular transcription profile (14, 15) and impairs the ability to mount a proper response to cellular stress. *Hmgn1*$^{tm1/tm1}$ mice and cells are hypersensitive to heat shock, and their ability to repair DNA damaged by either UV or ionizing radiation is impaired (16–19). Faulty repair of damaged DNA could lead to genomic instability and increased tumorigenicity. Taken together, the available information suggests that loss of HMGN1 may increase the susceptibility to tumorigenesis, a possibility that has not yet been fully examined.

Here we examine the potential role of HMGN1 in carcinogenesis, by comparing the progression of N-nitrosodiethylamine (DEN) induced hepatocarcinogenesis (20) in *Hmgn1*$^{tm1/tm1}$ mice and *Hmgn1*$^{+/+}$ littermates. DEN is a chemical carcinogen that has been extensively used for analysis of factors that affect liver cancer development, one of the most frequent human cancers (21). Young male mice are particularly susceptible to this carcinogen, as a single injection can result in hepatocellular carcinoma that is similar to that seen in humans (22). We find that loss of HMGN1 accelerates the development of liver cancers in DEN-injected mice. Transcription analysis of livers from these mice links loss of HMGN1 to alterations in several pathways including the sterol/ cholesterol/ lipid metabolic process, raising the possibility that transcriptional changes result in the accelerated carcinogenesis seen in *Hmgn1*$^{tm1/tm1}$ mice.

Materials and Methods

Animal studies

Hmgn1$^{tm1/tm1}$ (previously named *Hmgn1*$^{-/-}$) and control *Hmgn1*$^{+/+}$ mice were generated and genotyped as described (16). In these mice, exons II, III, and IV of the *Hmgn1* gene, which code for the nucleosome-binding domain of the protein, have been excised. For genotyping, tail DNA was extracted using REDExtract-N-Amp™ Tissue PCR Kit (Sigma-Aldrich) using three primers (see Supplementary Table S1). Since female mice are less sensitive than males to DEN-induced carcinogenesis, only male homozygous mice were used for the experiments. Mice received a single intraperitoneal (i.p.) injection of 10 μg/g body weight of N-nitrosodiethylamine (Sigma-Aldrich, Inc., Cat. 40334), or saline as a control, at 14 days of age. Mice were sacrificed at 23, 48, and 73 weeks after the injection. Animals were housed at the NCI Animal Facility and NCI-Frederick SAIC facility and cared for in accordance with the NIH Guide for the Care and Use of Laboratory Animals.

Necropsy and histopathology

All livers were harvested at necropsy, weighed, photographed and thoroughly examined. The number of macroscopic nodules/masses ≥1 mm was recorded for each liver. Livers were then fixed in 10% neutral buffered formalin, routinely processed to paraffin block, and sectioned at 5 μm. Hematoxylin-and-eosin (H&E) stained sections were evaluated microscopically for quantification of foci, adenomas, and carcinomas. The areas occupied by foci and neoplasms were measured using ImageJ software (NIH).

Protein isolation and Western blot analysis

Liver caudate lobes were homogenized by Dounce light homogenizer in 1×PBS. The cell suspensions were washed in 1×PBS and centrifuged at 600×g for 10 minutes. The cellular pellet was dissolved in either 0.2M sulfuric acid or 5% perchloric acid, both containing a protease inhibitor cocktail (Roche, Indianapolis, IN), homogenized by Dounce tight pestle homogenizer for 2 minutes, kept on ice for 5 minutes, and spun at 3,000×g for 10 minutes. The supernatant was made 25% in TCA, incubated on ice for 15 minutes, and centrifuged at 3,000×g for 20 minutes. The pellet was stored at −20°C overnight in 100% ethanol, air-dried, and re-suspended with 50 to 100 μl of water. The preparations were re-precipitated by HCl/acetone, washed in 100% acetone, air-dried, and re-suspended with 50 to 100 μl of water. Proteins were resolved on 15% Tris-glycine-SDS gels, transferred to polyvinylidene difluoride membrane, and subjected to Western blotting.

Immunohistochemistry staining

Immunohistochemical staining was carried out on formalin-fixed paraffin-embedded tissue using the avidin-biotin-peroxidase complex method (Vector Laboratories) and 3′-diaminobenzidine (DAB) for staining. Proliferating cell nuclear antigen antibody (PCNA; Santa Cruz Biotechnology, sc-25280) and rabbit anti-Ki67 antibody (Abcam, ab15580) were used according to the manufacturer's recommendation. Sections were counter-stained with hematoxylin.

RNA isolation

Total RNA was isolated from frozen liver tissue with TRIzol reagent (Invitrogen) followed by purification using RNeasy Kit (Qiagen) according to the manufacturer's instructions. Reverse transcription of total RNA (2.0 μg) into first strand cDNA using oligo(dT) primers (SuperScript First Strand Synthesis System for RT-PCR; Invitrogen) has been followed by PCR using Platinum PCR SuperMix (Invitrogen) and the specific primers (see Supplementary Table S1). PCR products were resolved on 2% agarose gels and visualized by ethidium bromide staining.

Microarray analysis

Expression profiling was conducted for six groups of mice. Group A consisted of mice at 4 weeks of age. Two other groups consisted of 12 week-old mice injected at the age of 4 weeks either with saline (group B) or DEN (group C). Each group includes both genotypes (*Hmgn1*$^{+/+}$ and *Hmgn1*$^{tm1/tm1}$).

For microarray analysis, total RNA was isolated as described above. The cDNA synthesis, fluorescent labeling of the samples, and mouse 430.2 Affymetrix expression array hybridizations were done following the suppliers recommendations. Arrays were scanned with Agilent scanner adjusted to achieve optimal signal intensity at both channels with <1% saturated spots and normalized to the 50th percentile of the median signal intensity. Normalized intensity values were used for further analysis.

Mouse Genome 430 2.0 array has 45101 probe sets associated with approximately 20 000 Mouse Genome Informatics (MGI) gene identifiers. Probe sets were mapped to MGI identifiers using information provided by the Jackson Laboratory (http://www.informatics.jax.org/). GeneSpring GX software package (Agilent Technologies) was employed to evaluate the quality of the arrays and for analysis.

Differentially expressed genes were selected using an univariate two-sample t test ($P \leq 0.01$) with a random variance model, using mean value for each of six groups (A-*Hmgn1*$^{+/+}$, A-*Hmgn1*$^{tm1/tm1}$, B-*Hmgn1*$^{+/+}$, B-*Hmgn1*$^{tm1/tm1}$, C-*Hmgn1*$^{+/+}$, C-*Hmgn1*$^{tm1/tm1}$). Unsupervised and supervised cluster analyses were done with GeneSpring GX analysis suite (version 11.5.1, Agilent Technologies, Cat. G3784AA). Functional GO and other data mining tools for significant genes were based on gene ontology annotations (Ingenuity Pathway Analysis software, Ingenuity Systems). The raw data for all 18 samples in can be found at GEO data set # GSE44356.

Quantitative real-time-PCR

Selected gene expression microarray data were confirmed by real-time qPCR using Applied Biosystems 7900 HT. Sequences of primers used for quantitative real-time-polymerase chain reaction (qRT-PCR) analyses are provided in Supplementary Table S1. GAPDH and actin primers were used for normalization of expression levels. qRT-PCR was performed using Power SYBR Green RNA-to-CT 1-Step Kit (Applied Biosystems, Cat. No 4391178) and iScript OneStep RT_PCR Kit with SYBR Green (Bio-Rad, Cat. No 170-8893) on a 7900HT Fast Real-Time PCR System instrument. A dissociation curve program was employed after each reaction. The purity of the PCR products was validated by electrophoresis on 4% NuSieve 3:1 agarose (Lonza, Rockland, ME).

RESULTS

HMGN1 affects the latency of DEN-induced hepatocarcinogenesis

To test whether loss of HMGN1 function affects the course of DEN-induced hepatocarcinogenesis, 2 week old male *Hmgn1*$^{+/+}$ and *Hmgn1*$^{tm1/tm1}$ littermate mice received a single intraperitoneal injection of N-nitrosodiethylamine at a dose of 10 μg/g body weight. Saline injected mice served as controls. Mice were sacrificed at ages of 25, 50 and 75 weeks and their livers examined for tumor incidence, size, multiplicity, and histological appearance. Western analysis of nuclear extracts from these livers indicated that during the course of the experiment the expression of HMGN1, or of its closely related protein HMGN2 did not change, and that in *Hmgn1*$^{tm1/tm1}$ mice, which lack nuclear HMGN1, there were no compensatory adjustment in the levels of HMGN2 (Figure 1).

As expected, the mice injected with DEN developed tumors, while the saline injected mice did not. We followed the development of the tumors by sacrificing mice 23, 48 and 73 weeks after DEN injection. At 23 weeks after DEN administration, the total number of preneoplastic foci observed in *Hmgn1*$^{tm1/tm1}$ mice was not significantly different from that observed in their *Hmgn1*$^{+/+}$ littermates; however, the size of the foci was significantly larger in *Hmgn1*$^{tm1/tm1}$ mice (Figure 2A). Thus, in *Hmgn1*$^{+/+}$ mice, 43% of the foci were smaller than 50 μM^2 and only 2% were larger than 500 μM^2, while in *Hmgn1*$^{tm1/tm1}$ mice less than 20% of the foci were smaller than 50 μM^2 and almost 30% of the foci were larger than 500 μM^2 (Figure 2A). Although the foci in *Hmgn1*$^{tm1/tm1}$ mice were larger, the rate of hepatocyte proliferation in the surrounding liver, as measured by mouse antigen Ki67 (Mki67) and PCNA immunostaining did not differ between the mice (Figure 3A). Likewise, although qRT-PCR analyses reveal the expected upregulation of cyclin D1 (Ccnd1), Mki67 and Myc, there were no significant differences between the DEN-injected *Hmgn1*$^{+/+}$ and

Hmgn1$^{tm1/tm1}$ littermate mice (Figure 3B). Comparative evaluation of H&E stained sections from the liver samples at 23 weeks after injection, indicated that in both *Hmgn1*$^{+/+}$ and *Hmgn1*$^{tm1/tm1}$ mice, the early pre-neoplastic lesions displayed a predominant basophilic cell phenotype characteristic of the DEN-induced carcinogenesis (Supplementary Figure S1).

In contrast, at 48 weeks post-DEN, both the number and size of pre-neoplastic and neoplastic lesions in *Hmgn1*$^{tm1/tm1}$ livers were considerably bigger than in *Hmgn1*$^{+/+}$ mice (Figure 2,B,C). The increased tumor frequency and size correlated with higher liver-to-body weight ratio, reflecting the apparent differences in the growth rate of pre-neoplastic and neoplastic hepatic lesions between knockout and control mice (Figure 2D). However at 75 week of age, no significant difference between *Hmgn1*$^{+/+}$ and *Hmgn1*$^{tm1/tm1}$ mice could be detected in any of the parameters of tumor growth examined, including liver-to-body weight ratios, tumor burden, and malignancy (Figure 2C, D). At this stage, the tumors were mostly hepatocellular adenomas and carcinomas, and the type of tumors observed was essentially the same in both wild type and *Hmgn1*$^{tm1/tm1}$ mice (Figure 2E). Thus, loss of HMGN1 enhances the rate of DEN-induced hepatocarcinogenesis but does not alter the type of tumors formed.

Effects of HMGN1 on the global gene expression pattern in the livers of DEN injected mice

To gain insights into the mechanisms whereby HMGN1 enhances the rate of tumorigenicity in the livers of DEN-injected mice, we examined the transcription profile in the livers of control and DEN injected *Hmgn1*$^{+/+}$ and *Hmgn1*$^{tm1/tm1}$ littermate mice. Since changes in gene expression would precede the appearance of preneoplastic foci and tumors, we examined the hepatic expression profiles in the following 3 groups, each consisting of 6 mice. The first group A which included 4-weeks old untreated *Hmgn1*$^{+/+}$ and *Hmgn1*$^{tm1/tm1}$ littermates served to test whether loss of HMGN1 affects the liver transcription profile prior to any treatment. The group B contained 12-weeks old *Hmgn1*$^{+/+}$ and *Hmgn1*$^{tm1/tm1}$ littermates that were injected with saline at 4 weeks of age. This group served as controls for group C, which consisted of 12 weeks old *Hmgn1*$^{+/+}$ and *Hmgn1*$^{tm1/tm1}$ littermates that were injected with DEN at 4 weeks of age. The raw data for all 18 samples can be found at GEO data set # GSE44356.

Principal Component Analysis (PCA) of the transcriptomes of all livers revealed a clear separation between the 3 groups (Fig 4A). The distinct clustering of group A from group B reflects the age-related changes in gene expression, while the distinct clustering of B from C reflects the DEN-induced changes in gene expression. Within each group, the *Hmgn1*$^{+/+}$ mice formed a subcluster that was separate from their *Hmgn1*$^{tm1/tm1}$ littermates, the largest difference between these subclusters was observed in the youngest mice (group A). Supervised comparison based on asymptotic one-way ANOVA calculation using a P value ≤ 0.01 revealed that in total the expression of 2654 genes was altered. Of these, the expression of 520 genes was altered more than two-fold between at least two groups (Supplementary Table S2). The microarray expression data were validated by real-time PCR of 8 genes randomly selected in Group A, using two sets of primers per each gene (Figure 4B).

Venn diagrams of the up- and downregulated genes revealed a partial overlap between the 3 groups (Figure 4C). We note that the total number of genes which expression changed due to lack of HMGN1 was similar among the 3 groups. Thus, in the 4-week old untreated mice (Group A), loss of HMGN1 led to the upregulation of 172 genes and downregulation of 152 genes; a total change of 324 genes. Similarly, the total number of genes changed in group B and C was 322 and 334, respectively. Examination of the ten top genes which expression was either up or down regulated in each group (Table 1) did not reveal common genes or pathways regulated by HMGN1. Likewise, it did not contain any genes that could likely contribute to shorten the latency or tumorigenicity. The partial overlap between the genes

down regulated in groups B and C suggests that the effect were due to loss of HMGN1 rather than to DEN treatment. The data are consistent with previous findings that HMGN1 alters slightly the expression of numerous genes but does not specifically regulate the expression of a distinct subset of genes (14, 15).

Hierarchical clustering defines groups of genes associated with DEN- induced altered expression patterns

Hierarchical condition tree of unsupervised clustering analysis of the differentially expressed genes (n=520, FC≥2, P≤0.01)) sorted apart groups A, B and C (top of the heat map), without separating between two genotypes in each group (Figure 5A). Using a threshold distance of 0.25 on the Y-axis dendrogram, the genes were classified into 8 major clusters, each representing a specific gene expression pattern (green boxes C1–C8, Figure 3A). The overall pattern of clustering revealed that the differences between groups A,B, and C, were larger than the differences between the *Hmgn1*$^{+/+}$ and *Hmgn1*$^{tm1/tm1}$ within each group, a further indication that loss of HMGN1 does not have a major impact on the expression levels of a specific subset of genes. Nevertheless, clusters C2, C3, C7 and C8 contained the subsets of genes affected by the loss of HMGN1. Thus, in *Hmgn1*$^{tm1/tm1}$ mice, the genes in clusters C2,C3 and part of C4 were downregulated, the genes in clusters C7 and C8 were upregulated. The differences between groups B and C were the most prominent in clusters C4, C5, and C6; these genes may be involved in the liver response to DEN injection.

A search for the genes linked to hyper-proliferation, dysplasia and other cancer-related genes in the various groups and clusters yielded *JunB.* This was the only cancer-related gene which was overexpressed in *Hmgn1*$^{tm1/tm1}$ mice at 4 weeks of age but not following DEN administration at 12 weeks, making it unlikely to contribute to the difference in tumor development at the later stages. Likewise, of the 65 genes associated with high risk of poor prognosis for hepatocellular carcinoma (23) only the *Tbx3* transcription factor was differentially expressed in *Hmgn1*$^{tm1/tm1}$ livers, but its expression was down-regulated. These results further support the notion that HMGN1 does not specifically regulate the expression of genes involved in liver carcinogenesis.

Functional analysis of all 520 differentially expressed genes identified the sterol/ cholesterol/ lipid metabolic process pathway-associated genes as the most altered (*P*≤4.09E-05) (Supplementary Table S3). Similar analysis of the 8 gene clusters identified by unsupervised clustering analysis (Figure 5A) revealed that the sterol/ cholesterol/ lipid metabolic process pathway-associated genes were most significantly over-represented (*P*≤3.14E-12) in cluster C2 (Figure 5B). This cluster contained several genes belonging to this pathway including *Fasn, Cyp7a1, Mvd,* and *Thrsp* (Figure 5B). In addition, in cluster C6, the presence of transcription factor activity pathway-oriented genes GO:0006366 presence is highly enriched (*P*≤1.23E-8). This cluster contained genes that were upregulated by DEN treatment and differed between *Hmgn1*$^{+/+}$ and *Hmgn1*$^{tm1/tm1}$ littermates (Figure 5B) and could contribute to earlier signs of DEN-induced hepatocarcinogenesis which we observed in *Hmgn1*$^{tm1/tm1}$ mice.

Discussion

In the present study we show that loss of HMGN1 protein in mice increases the rate of liver tumorigenesis after DEN treatment. In *Hmgn1*$^{tm1/tm1}$ mice pre-neoplastic lesions seen at 23 weeks after DEN-administration were larger than in the *Hmgn1*$^{+/+}$ littermates. Likewise, the number of foci, and the average size of tumors seen was significantly increased in the 50 week old mice lacking functional HMGN1 protein as compared to wild type mice. However, at 73 weeks after DEN administration, the size and number of tumors, and their histological

appearance were similar in both *Hmgn1*$^{+/+}$ and *Hmgn1*$^{tm1/tm1}$ mice. Thus, loss of HMGN1 increased the growth rate, but not the type of tumors or the tumor burden.

The results are compatible with previous findings of increased tumor incidence in *Hmgn1*$^{tm1/tm1}$ mice suggesting that loss of HMGN1 predisposes to increased tumor susceptibility (17). Embryonic fibroblasts from *Hmgn1*$^{tm1/tm1}$ mice were shown to proliferate faster than cells prepared from their *Hmgn1*$^{+/+}$ littermates, and SV40-immortalized *Hmgn1*$^{tm1/tm1}$ cells induced more tumors than SV40-transformed *Hmgn1*$^{+/+}$ cells when injected into nude mice (17). In addition, HMGN1 increased the recruitment rate of proliferating cell nuclear antigen (PCNA) to UV-damaged DNA sites (24) and loss of HMGN1 impaired the ability of *Hmgn1*$^{tm1/tm1}$ cells to repair DNA damaged by either UV or ionizing irradiation (16, 17, 25), thereby predisposing *Hmgn1*$^{tm1/tm1}$ mice to increased genomic instability and tumorigenicity (17, 26). In agreement with these findings (17, 26), the cancer initiation was notably faster in *Hmgn1*$^{tm1/tm1}$ mice treated with DEN. However at the later stages, the differences in DEN-induced tumor development between *Hmgn1*$^{+/+}$ and *Hmgn1*$^{tm1/tm1}$ mice became less pronounced suggesting the differential requirements for HMGN1 function during multistep process of chemical hepatocarcinogenesis. As we have shown in the past, several proto-oncogenes, such as JunB and c-Jun, have been down-regulated in the *Hmgn1*$^{tm1/}$tm1 fibroblasts (9). Thus, HMGN1 regulates the transcription of multiple genes which may have opposing effects on the rate of tumor growth at different stages of tumor development.

Our analysis of the liver transcription profiles did not reveal significant effect of HMGN1 deletion on the expression levels of DNA damage repair factors suggesting that the accelerated hepatocarcinogenesis in *Hmgn1*$^{tm1/tm1}$ is not due to faulty expression of these factors. In agreement with previous analyses of a variety of tissues including liver, loss of HMGN disrupted the expression of multiple genes but only mildly, suggesting that HMGN1 fine tunes the fidelity of the cellular transcription profile (14, 15). DEN injection did not significantly increase the transcription differences between *Hmgn1*$^{+/+}$ and *Hmgn1*$^{tm1/tm1}$ mice, a finding that is fully compatible with the similarity in the number and types of tumors seen in the mice. Thus loss of HMGN1 does not fundamentally alter the cellular response to DEN.

GO analysis identified the sterol/ lipid metabolic pathways as the most different category of genes between DEN injected *Hmgn1*$^{+/+}$ and *Hmgn1*$^{tm1/tm1}$ mice. Emerging evidence links altered sterol/ lipid metabolic profile to chronic low-grade systemic inflammation (27), which is believed to contribute to metabolic disorders, and the stagewise progression to hepatic steatosis, fibrosis, cirrhosis, and finally to carcinoma (28–30). Hepatocellular carcinoma has been also linked to non-alcoholic fatty liver disease (31). As an architectural element of chromatin, HMGN1 protein is capable to change expression profile of the cell globally, affecting several pathways simultaneously (14, 15).

Supplementary Material

Refer to Web version on PubMed Central for supplementary material.

Acknowledgments

The research was supported by the Center for Cancer Research, The Intramural Research Program at the National Institutes of Health, National Cancer Institute, and with funds from the National Cancer Institute, National Institutes of Health, under Contract No. HHSN261200800001E. We thank the NIH Library Writing Center, Bethesda, MD for editorial help.

NCI-Frederick is accredited by AAALAC International and follows the Public Health Service Policy for the Care and Use of Laboratory Animals. Animal care was provided in accordance with the procedures outlined in the

"Guide for Care and Use of Laboratory Animals" (National Research Council; 1996; National Academy Press; Washington, D.C.)

References

1. Esteller M. Cancer epigenomics: DNA methylomes and histone-modification maps. Nat Rev Genet. 2007; 8:286–98. [PubMed: 17339880]
2. Murrell A, Hurd PJ, Wood IC. Epigenetic Mechanisms in Development and Disease. Biochem Soc Trans. 2013; 41:697–9. [PubMed: 23697928]
3. Garraway LA, Lander ES. Lessons from the cancer genome. Cell. 2013; 153:17–37. [PubMed: 23540688]
4. Jones PA, Baylin SB. The epigenomics of cancer. Cell. 2007; 128:683–92. [PubMed: 17320506]
5. Dawson MA, Kouzarides T. Cancer epigenetics: from mechanism to therapy. Cell. 2012; 150:12–27. [PubMed: 22770212]
6. Bustin M. Chromatin unfolding and activation by HMGN(*) chromosomal proteins. Trends Biochem Sci. 2001; 26:431–7. [PubMed: 11440855]
7. Catez F, Lim JH, Hock R, Postnikov YV, Bustin M. HMGN dynamics and chromatin function. Biochem Cell Biol. 2003; 81:113–22. [PubMed: 12897844]
8. Cuddapah S, Schones DE, Cui K, Roh TY, Barski A, Wei G, et al. Genomic profiling of HMGN1 reveals an association with chromatin at regulatory regions. Mol Cell Biol. 2011; 31:700–9. [PubMed: 21173166]
9. Lim JH, Catez F, Birger Y, West KL, Prymakowska-Bosak M, Postnikov YV, et al. Chromosomal protein HMGN1 modulates histone H3 phosphorylation. Mol Cell. 2004; 15:573–84. [PubMed: 15327773]
10. Lim JH, West KL, Rubinstein Y, Bergel M, Postnikov YV, Bustin M. Chromosomal protein HMGN1 enhances the acetylation of lysine 14 in histone H3. EMBO J. 2005; 24:3038–48. [PubMed: 16096646]
11. Postnikov YV, Belova GI, Lim JH, Bustin M. Chromosomal protein HMGN1 modulates the phosphorylation of serine 1 in histone H2A. Biochemistry. 2006; 45:15092–9. [PubMed: 17154547]
12. Ueda T, Postnikov YV, Bustin M. Distinct domains in high mobility group N variants modulate specific chromatin modifications. J Biol Chem. 2006; 281:10182–7. [PubMed: 16484217]
13. Kim YC, Gerlitz G, Furusawa T, Catez F, Nussenzweig A, Oh KS, et al. Activation of ATM depends on chromatin interactions occurring before induction of DNA damage. Nat Cell Biol. 2009; 11:92–6. [PubMed: 19079244]
14. Kugler JE, Horsch M, Huang D, Furusawa T, Rochman M, Garrett L, et al. High Mobility Group N Proteins Modulate the Fidelity of the Cellular Transcriptional Profile in a Tissue- and Variant-specific Manner. J Biol Chem. 2013; 288:16690–703. [PubMed: 23620591]
15. Rochman M, Taher L, Kurahashi T, Cherukuri S, Uversky VN, Landsman D, et al. Effects of HMGN variants on the cellular transcription profile. Nucleic Acids Res. 2011; 39:4076–87. [PubMed: 21278158]
16. Birger Y, West KL, Postnikov YV, Lim JH, Furusawa T, Wagner JP, et al. Chromosomal protein HMGN1 enhances the rate of DNA repair in chromatin. EMBO J. 2003; 22:1665–75. [PubMed: 12660172]
17. Birger Y, Catez F, Furusawa T, Lim JH, Prymakowska-Bosak M, West KL, et al. Increased tumorigenicity and sensitivity to ionizing radiation upon loss of chromosomal protein HMGN1. Cancer Res. 2005; 65:6711–8. [PubMed: 16061652]
18. Belova GI, Postnikov YV, Furusawa T, Birger Y, Bustin M. Chromosomal protein HMGN1 enhances the heat shock-induced remodeling of Hsp70 chromatin. J Biol Chem. 2008; 283:8080–8. [PubMed: 18218636]
19. Fousteri M, Vermeulen W, van Zeeland AA, Mullenders LH. Cockayne syndrome A and B proteins differentially regulate recruitment of chromatin remodeling and repair factors to stalled RNA polymerase II in vivo. Mol Cell. 2006; 23:471–82. [PubMed: 16916636]

20. Dragan YP, Xu YH, Pitot HC. The effect of the dose of diethylnitrosamine on the initiation of altered hepatic foci in neonatal female rats. Carcinogenesis. 1993; 14:385–91. [PubMed: 8095861]
21. Soerjomataram I, Lortet-Tieulent J, Parkin DM, Ferlay J, Mathers C, Forman D, et al. Global burden of cancer in 2008: a systematic analysis of disability-adjusted life-years in 12 world regions. Lancet. 2012; 380:1840–50. [PubMed: 23079588]
22. Verna L, Whysner J, Williams GM. N-nitrosodiethylamine mechanistic data and risk assessment: bioactivation, DNA-adduct formation, mutagenicity, and tumor initiation. Pharmacol Ther. 1996; 71:57–81. [PubMed: 8910949]
23. Kim SM, Leem SH, Chu IS, Park YY, Kim SC, Kim SB, et al. Sixty-five gene-based risk score classifier predicts overall survival in hepatocellular carcinoma. Hepatology. 2012; 55:1443–52. [PubMed: 22105560]
24. Postnikov YV, Kurahashi T, Zhou M, Bustin M. The nucleosome binding protein HMGN1 interacts with PCNA and facilitates its binding to chromatin. Mol Cell Biol. 2012; 32:1844–54. [PubMed: 22393258]
25. Subramanian M, Gonzalez RW, Patil H, Ueda T, Lim JH, Kraemer KH, et al. The nucleosome-binding protein HMGN2 modulates global genome repair. FEBS J. 2009; 276:6646–57. [PubMed: 19843163]
26. Gerlitz G. HMGNs, DNA repair and cancer. Biochim Biophys Acta. 2010; 1799:80–5. [PubMed: 20004154]
27. Vongsuvanh R, George J, Qiao L, van der Poorten D. Visceral adiposity in gastrointestinal and hepatic carcinogenesis. Cancer Lett. 2013; 330:1–10. [PubMed: 23201597]
28. Jou J, Choi SS, Diehl AM. Mechanisms of disease progression in nonalcoholic fatty liver disease. Semin Liver Dis. 2008; 28:370–9. [PubMed: 18956293]
29. Szabo G, Lippai D. Molecular hepatic carcinogenesis: impact of inflammation. Dig Dis. 2012; 30:243–8. [PubMed: 22722548]
30. Sun B, Karin M. Obesity, inflammation, and liver cancer. J Hepatol. 2012; 56:704–13. [PubMed: 22120206]
31. Starley BQ, Calcagno CJ, Harrison SA. Nonalcoholic fatty liver disease and hepatocellular carcinoma: a weighty connection. Hepatology. 2010; 51:1820–32. [PubMed: 20432259]

Implications

Loss of HMGN1 leads to accelerated progression of DEN-induced hepatocarcinogenesis in mice.

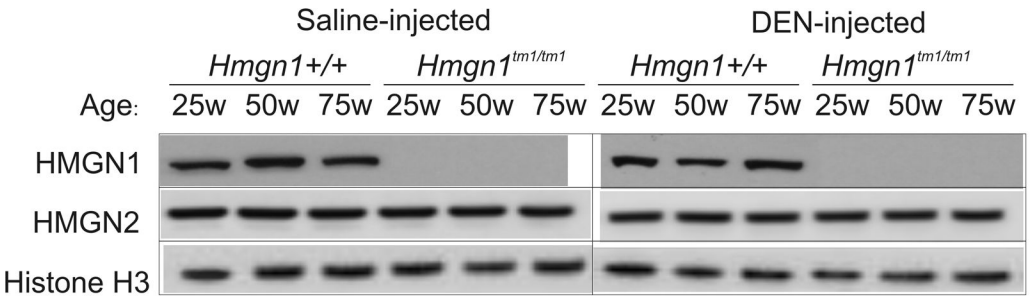

Figure 1. Expression of HMGN1 and HMGN2 during the course of the experiment

Shown are Western blotting analyses of HMGN1, HMGN2 and histone H3 in livers of 25-, 50- and 75-week-old *Hmgn1*$^{+/+}$ and *Hmgn1*$^{tm1/tm1}$ mice which were injected with either DEN or saline at 2 weeks of age.

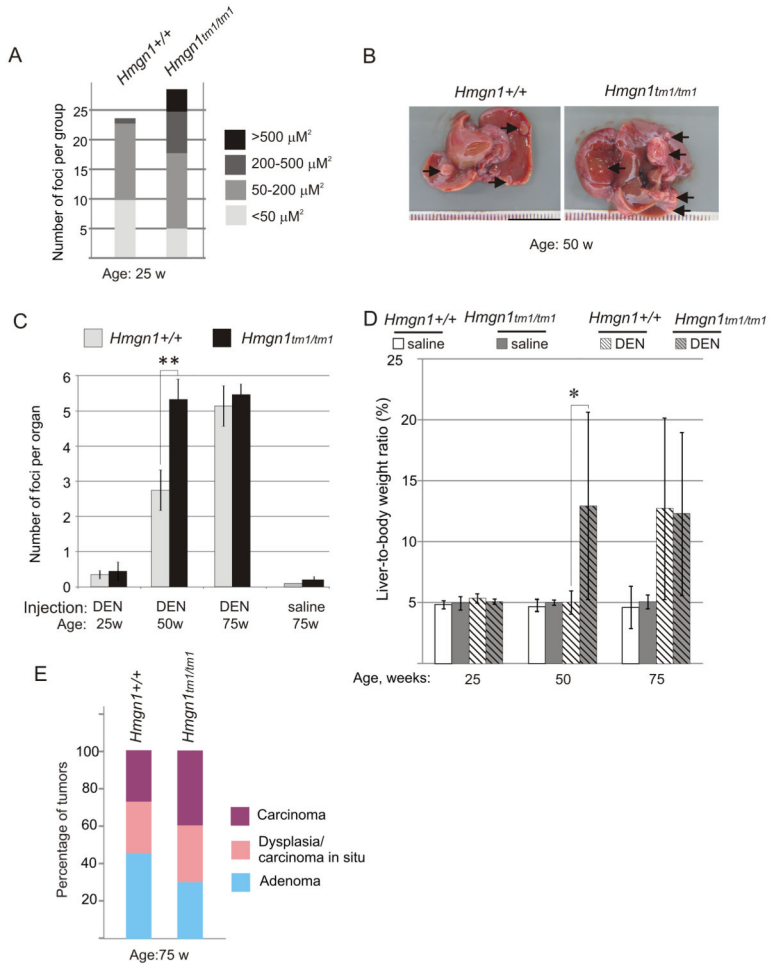

Figure 2. Incidence and kinetics of growth of liver tumors in DEN–treated H*mgn1*$^{+/+}$ and *Hmgn1*$^{tm1/tm1}$ mice

A. Size distribution of hepatic lesions in DEN-injected *Hmgn1*$^{+/+}$ and *Hmgn1*$^{tm1/tm1}$ mice at 25 weeks. Areas of the foci have been determined using ImageJ software. **B.** Representative images of livers from 50 weeks old DEN-injected *Hmgn1*$^{+/+}$ and *Hmgn1*$^{tm1/tm1}$ mice. Tumors are indicated by arrows. **C.** Kinetics of tumor incidence in livers from DEN-treated *Hmgn1*$^{+/+}$ and *Hmgn1*$^{tm1/tm1}$ mice. ** $P \leq 0.01$, determined by Fisher's test, . **D.** Liver to whole body weight ratios of 25, 50 and 75 weeks old *Hmgn1*$^{+/+}$ and *Hmgn1*$^{tm1/tm1}$ mice after saline- or DEN-treatment (*$P \leq 0.05$). **E.** Histograms of tumor types in livers of 75 week old DEN injected mice.

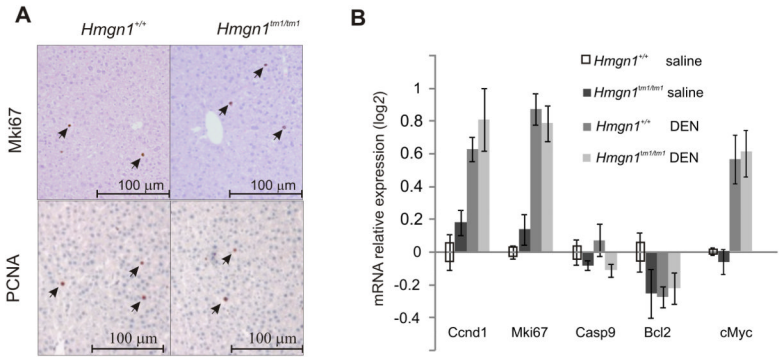

Figure 3. Apoptotic and proliferative activity in livers of *Hmgn1*$^{+/+}$ and *Hmgn1*$^{tm1/tm1}$ mice, 23 weeks after DEN injection

A. Representative light microscopy images of immunoperoxidase staining with Mki67 (upper images) and PCNA (bottom images) of paraffin-embedded liver sections counterstained with hematoxylin. Positively-stained cells are indicated by arrows. **B**. Relative mRNA expression levels of genes involved in control of proliferation (cyclin D1 and Ki-67) and apoptosis (caspase-9 and Bcl2) as measured by qRT-PCR (3 mice per saline-injected and DEN-injected group of mice of each genotype). The data are ΔΔCt values (mean ± S.E.M.). The expression levels were normalized to that of saline-injected *Hmgn1*$^{+/+}$ mice, which was set to 1.

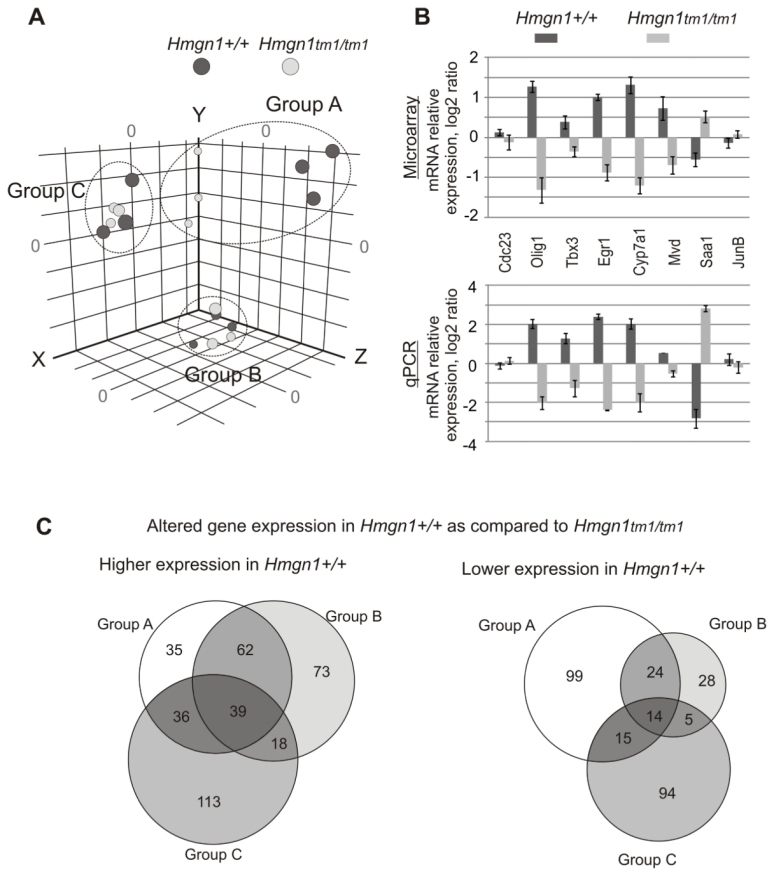

Figure 4. Effects of HMGN1 on gene expression in livers

A. Principal Component Analysis of the transcription profiles in the livers of control and DEN-injected *Hmgn1*$^{+/+}$ and *Hmgn1*$^{tm1/tm1}$ livers. Each dot represents one mouse. The size of the dot reflects its position within the 3D plot. **B.** Validation of microarray data by semi-quantitative PCR. Microarray data are represented by logarithm base 2 ratios of the average individual entity (gene) intensities for *Hmgn1*$^{+/+}$ and *Hmgn1*$^{tm1/tm1}$ mice (three mice of each genotype, non-treated by DEN at 4 weeks of age) and normalized for the total intensity (GeneSpring GX 11.5.1 by Agilent Technologies). Ratios based on RT-PCR data were calculated in a way to be compared to microarray data (comparative Ct method). ΔCt value was calculated for each primer set normalized to control primers (GAPDH and β-actin) for every biological sample. Next, the values were converted into relative amount of target by using a formula *Normalized amount of specific mRNA* = $2^{\Delta\Delta Ct}$. Normalized amounts of mRNAs were plotted as log 2 ratio between wild-type and mutant samples. **C**. Venn diagrams of up - and down -regulated genes in the 3 groups investigated. Group A: 4-week untreated *Hmgn1*$^{+/+}$ and *Hmgn1*$^{tm1/tm1}$ littermates. Group B: 12 weeks old littermates injected with saline at 4 weeks of age. Group C: 12 weeks old littermates injected with DEN at 4 weeks of age.

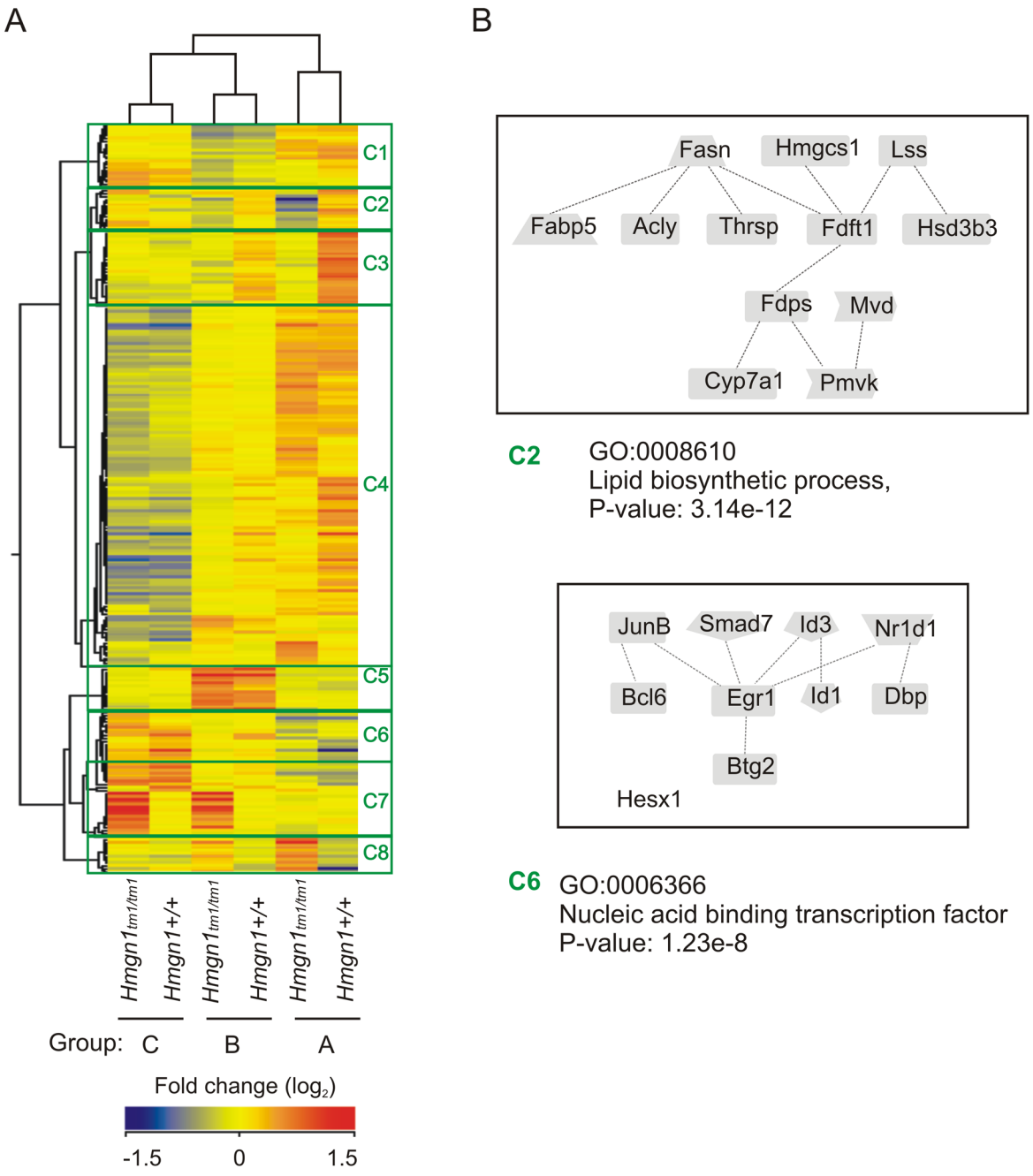

Figure 5. Functional classification of the differentially expressed genes in livers of *Hmgn1*$^{+/+}$ and *Hmgn1*$^{tm1/tm1}$ mice before and after DEN or saline injection

A. Heat map describing the clustering of the expression profile of the differentially expressed genes (n=520, FC≥2, P≤0.01). The conditional tree on top of the heat map, which sorted the genes into groups A, B and C, was generated by unsupervised clustering analysis. Groups C1–C8 were generated using a threshold distance of 0.25 on the Y-axis dendrogram. **B.** Network analysis of genes in the two most affected GO pathways in the livers of *Hmgn1*$^{tm1/tm1}$ mice. Shown are the networks of the genes in the lipid metabolism pathway (cluster 2 of Fig. 5A) and in transcription factors pathway (cluster 6 of Fig. 5A) generated by GePS pathway analysis (Genomatix Software GmbH).

Table 1

Top ten genes, differentially expressed in livers of *Hmgn1*$^{+/+}$ and *Hmgn1*$^{tm1/tm1*}$ mice

Genes, up-regulated in *Hmgn1*$^{+/+}$								
Group A			**Group B**			**Group C**		
Gene Symbol	**Entrez Gene**	**Expression log2 ratio, *Hmgn1*$^{+/+}$ vs. *Hmgn1*$^{-/-*}$)**	**Gene Symbol**	**Entrez Gene**	**Expression log2 ratio, *Hmgn1*$^{+/+}$ vs. *Hmgn1*$^{-/-}$)**	**Gene Symbol**	**Entrez Gene**	**Expression log 2 ratio, *Hmgn1*$^{+/+}$ vs. *Hmgn1*$^{-/-}$)**
Cyp7a1	13122	2.56	Xlr4a	434794	1.46	Myh1	17879	1.18
Olig1	50914	2.40	Cyp7a1	13122	1.20	Creld2	22059	1.02
Acta2	11475	1.61	Olig1	50914	1.16	Dbp	13170	0.92
Pltp	18830	1.58	Mvd	192156	1.04	Tff3	21786	0.90
Cdk5rap1	66971	1.54	Rgs16	19734	1.01	Mt2	17750	0.84
Naip2	17948	1.54	Hspa8	15481	0.95	Scara5	71145	0.80
Mvd	192156	1.52	Ccdc25	67179	0.94	Syvn1	74126	0.71
Hspa8	15481	1.51	Fasn	14105	0.91	Mt1	17748	0.70
Fabp5	16592	1.51	Thrsp	21835	0.90	Mtss1	211401	0.63
Hhex	15242	1.48	BC005512	192885	0.88	Onecut1	15379	0.60

Genes, down-regulated in *Hmgn1*$^{+/+}$								
Group A			**Group B**			**Group C**		
Gene Symbol	**Entrez Gene**	**Expression log2 ratio, *Hmgn1*$^{+/+}$ vs. *Hmgn1*$^{-/-}$)**	**Gene Symbol**	**Entrez Gene**	**Expression log2 ratio, *Hmgn1*$^{+/+}$ vs. *Hmgn1*$^{-/-}$)**	**Gene Symbol**	**Entrez Gene**	**Expression log 2 ratio, *Hmgn1*$^{+/+}$ vs. *Hmgn1*$^{-/-}$)**
Scara5	71145	−3.52	Hsd3b1	15492	−2.20	Hsd3b1	15492	−2.15
Mt2	17750	−3.12	Star	20845	−2.08	Star	20845	−2.03
Id1	15901	−2.73	Akr1b7	11997	−2.02	Akr1b7	11997	−1.95
Mt1	17748	−2.43	Chgb	12653	−1.70	Adipoq	9370	−1.88
Slc15a2	57738	−2.24	Adipoq	9370	−1.69	Scg2	20254	−1.78
Id2	15902	−2.15	Id1	15901	−1.55	Cyp11b1	110115	−1.73
Dbp	13170	−1.94	Cyp11b1	110115	−1.45	Chga	12652	−1.71
Skiv2l2	72198	−1.77	Id2	15902	−1.37	Chgb	12653	−1.66
Egr1	13653	−1.74	Bcl6	12053	−1.36	Cyp11a1	13070	−1.62
Hes1	15205	−1.64	Scg2	20254	−1.30	Hao2	56185	−1.52

*In the table the *Hmgn1*$^{tm1/tm1}$ genotype is indicated as *Hmgn1*$^{-/-}$